# Modelling of Boundary Layer Stability

by

## Paul Andersson

December 1999
Technical Reports from
Royal Institute of Technology
Department of Mechanics
S-100 44 Stockholm, Sweden

Typsatt i  $\mathcal{AMS}$ - $\mathbb{A}T_{E}X$ .

Akademisk avhandling som med tillstånd av Kungliga Tekniska Högskolan i Stockholm framlägges till offentlig granskning för avläggande av teknologie doktorsexamen torsdagen den 16 december 1999 kl 10.15 i Kollegiesalen, Administrationsbyggnaden, Kungliga Tekniska Högskolan, Valhallavägen 79, Stockholm.

©Paul Andersson 1999 Norstedts Tryckeri AB, Stockholm 1999

#### Modelling of Boundary Layer Stability

#### Paul Andersson 1999

Department of Mechanics, Royal Institute of Technology S-100 44 Stockholm, Sweden

#### Abstract

A scenario for bypass transition to turbulence likely to occur in natural transition in a flat plate boundary layer flow has been studied. The exponential growth or decay of two-dimensional wave disturbances, known as Tollmien-Schlichting waves, has long been the classical starting point for theoretical investigations of transition from laminar to turbulent flow. Its failure to explain experimentally observed transition for many flows has attracted intense interest to the recently revealed existence of non-modal growth mechanisms. This thesis focus mainly on transition emanating from the non-modal transient growth of streamwise streaks. Streamwise streaks are ubiquitous in transitional boundary layers, particularly when subjected to high levels of free-stream turbulence. The upstream disturbances experiencing maximum spatial energy growth have been calculated numerically using techniques commonly employed when solving optimal-control problems for distributed parameter systems. The calculated optimal disturbances consist of streamwise aligned vortices developing downstream into streamwise streaks which are in good agreement with experimental measurements. The maximum spatial energy growth was found to scale linearly with the distance from the leading edge. Based on these results, a simple model for prediction of transition location is proposed. However, the non-modal growth of streamwise streaks only represent the initial phase of transition. If the disturbance energy of the streaks becomes sufficiently large, secondary instabilities can take place and provoke early breakdown and transition, overruling the theoretically predicted modal decay. Using linear Floquet theory the temporal, inviscid secondary instability of these streaks were studied to determine the characteristic features of their breakdown. The critical streak amplitude beyond which streamwise travelling waves are excited is typically of order 26% of the free-stream velocity. The sinuous secondary instability mode was found to represent the most dangerous symmetry for travelling disturbances. Also the numerical-stability consequences of the remaining ellipticity in the Parabolic Stability Equations (PSE) are studied. The equations are found to constitute an ill-posed Cauchy problem. Suggestions of how to make the equations well-posed and to remove the methods otherwise intrinsic step-size restriction are given.

**Descriptors:** laminar-turbulent transition, boundary layer flow, non-parallel effects, adjoint equations, transient growth, optimal disturbances, streamwise streaks, streak instability, secondary instability, transition modelling, free-stream turbulence, parabolic stability equations, ill-posed equations.

## Preface

This thesis considers the stability of boundary layer flows and modelling aspects. The thesis is based on and contains the following papers.

- **Paper 1.** Andersson, P., Henningson, D. S. & Hanifi, A. 1998 On a stabilization procedure for the parabolic stability equations. *J. Eng. Math.* 33, 311–332.
- **Paper 2.** Andersson, P., Berggren, M. & Henningson, D. S. 1999 Optimal disturbances and bypass transition in boundary layers. *Phys. Fluids* 11, 134–150.
- **Paper 3.** Andersson, P., Brandt, L., Bottaro, A. & Henningson, D. S. 1999 On the breakdown of boundary layer streaks. *submitted to J. Fluid Mech.*
- Paper 4. Andersson, P., Bottaro, A., Henningson, D. S. & Luchini, P. 1999 Secondary instability of boundary layer streaks based on the shape assumption. TRITA-MEK, Technical Report 1999:13, Dept. of Mechanics, KTH, Stockholm, Sweden.
- **Paper 5.** Andersson, P. 1999 On the modelling of streamwise streaks in the Blasius boundary layer. TRITA-MEK, Technical Report 1999:14, Dept. of Mechanics, KTH, Stockholm, Sweden.

The papers are here re-set in the present thesis format, and some minor corrections have been made as compared to published versions. The first part of the thesis is both a short introduction to the field and a summary of the most important results presented in the papers given above.

# Contents

Preface		iv
Chapter 1. I	$\operatorname{ntroduction}$	1
Chapter 2. (	Overview of transition history	3
2.1. Reyne	olds classical experiment	3
2.2. Class	ical linear stability theory	3
2.3. Squir	e's theorem and the role of three-dimensionality	5
Chapter 3. S	patially evolving disturbances and non-parallel effects	6
3.1. Spati	al stability and non-parallel effects	6
3.2. The I	Parabolised Stability Equations	6
Chapter 4. N	Non-modal amplification	10
4.1. Lift-u	p and transient growth	10
4.2. Optin	nal disturbances	11
4.2.1. 7	Temporal setting	11
4.2.2. S	patial setting	12
Chapter 5. S	econdary instability	18
5.1. Satur	ation and general introduction of secondary instability	18
5.2. Secon	dary instability of two-dimensional waves	19
5.3. Secon	dary instability of streaks	20
5.4. Obliq	ue transition	25
Chapter 6. T	Cransition modelling for high free-stream turbulence levels	26
6.1. "Clas	sical" empirical correlations	26
6.2. Mode	el based on the $e^N$ -method	26
6.3. Trans	sition prediction based on non-modal amplification	27
f Acknowledgen	nents	29
Bibliography		30
Paper 1. On	a stabilization procedure for the parabolic stability equations	37
Paper 2. Opt	timal disturbances and bypass transition in boundary layers	63

v

Paper 3.	On the breakdown of boundary layer streaks	103
Paper 4.	Secondary instability of boundary layer streaks based on the shape assumption	e 145
Paper 5.	On the modelling of streamwise streaks in the Blasius boundary layer	169

### Introduction

Sleepless for over 24 hours and awaiting my transfer flight to take me home to Stockholm from San Francisco, I saw a five-year-old boy reaching out and trying to grip a miniature cyclone on display at Frankfurt airport. While we both watched as the water aerosol smoke slipped away between his fingers I experienced a moment of basic understanding from where the fascination for fluid mechanics arises. It appears as a ghost from nowhere and makes leaves move in strange patterns. The fog rolls in at night, seemingly from nowhere. Much like modern times fascination for black holes we often do not notice the actual fluid but only its effect on other matter. And as I realized that evening, most important; "It slips through your fingers impossible to grasp".

The child, the engineer, the applied mathematician, and even the not—so—applied mathematician can all share the feeling of being unable to grasp the phenomena occurring in a fluid flow. Even though the governing equations have been around for almost two hundred years only a handful of solutions to practical problems are known to man. From a theoretical point of view the uniqueness and regularity of solutions in three space dimensions is still an open question and from a practical standpoint the methods of finding approximate solutions are still not satisfactory enough for many applications.

This situation creates a need for simplified models based on careful approximations of the Navier–Stokes equations together with a deep physical insight, often gained from experimental observations of a related flow configuration. This thesis is concerned with a number of such models, all describing different aspects of the fluid mechanics phenomenon denoted *transition*.

The term transition refers to the passage between two states of fluid flows: the ordered, regular, and predictable laminar flow as opposed to the swirly, fluctuating, and chaotic turbulent flow. The transition process itself is usually further divided into three different stages. The receptivity stage, where the disturbance is introduced and established into the flow. The stability phase concerns the development of the established disturbance in time (temporal) or in space (spatial). Of course the aspect of major interest is whether the disturbance is growing or decaying depending on its characteristics. The last phase is the subsequent nonlinear breakdown of the growing disturbances which is characterised by nonlinear generation of a multitude of scales which represent the typical characteristic of a turbulent flow.

1

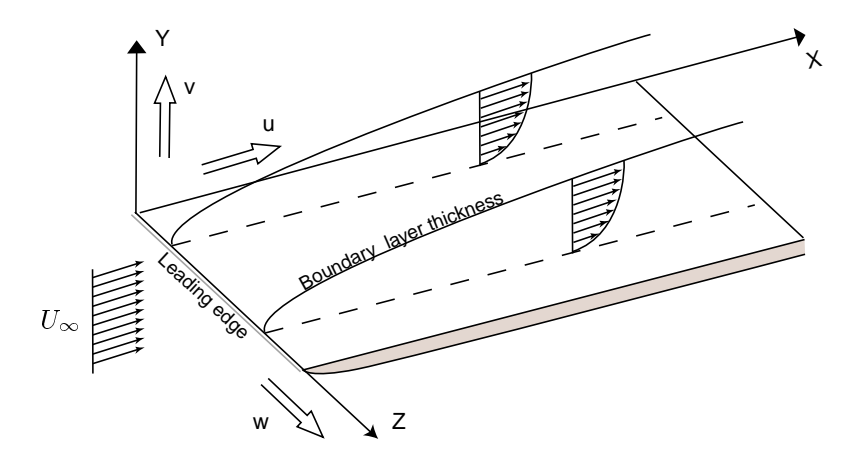


FIGURE 1.1 Flat plate boundary layer flow with free-stream velocity  $U_{\infty}$ . The coordinate system has directions x, y and z with corresponding velocity components u, v and w.

The present thesis deals with the stability and breakdown stages of transition inside a boundary layer which forms over a flat plate when subjected to a uniform oncoming flow field (see figure 1.1). The boundary layer is established due to viscosity. This internal friction forces the velocity from its free-stream value a distance above the wall to zero immediately at the surface.

At vehicles travelling through air the typical thickness of a boundary layer is quite small. A typical value of the boundary layer thickness one meter in on a motor-hood of a car travelling at  $100 \, \mathrm{km/h}$  is about one millimeter, unless, of course, your Mercedes star has provoked early transition; in which case the value would be slightly larger.

## Overview of transition history

#### 2.1. Reynolds classical experiment

In the classical pioneering work of Osborne Reynolds [58] (1883), he studies the transition process in the shear flow inside a glass tube. By injecting colour at the centreline in the inlet of the pipe he could visualise the shift from the ordered laminar motion to the irregular turbulent motion. He writes: "When the velocities were sufficiently low the colour extended in a beautiful straight line through the tube". However, at higher velocities the straight line became irregular and was mixed with the surrounding fluid in a violent way. Increasing the velocity further shortened the distance between the inlet and the point where the transition to turbulence started. By varying a number of different flow parameters, including the pipe radius, r, the kinematic viscosity of the fluid,  $\nu$ , and the bulk velocity, U, he found that when the non-dimensional quantity that later became known as the Reynolds number,  $Re = Ur/\nu$ , exceeded a threshold value the flow became unstable. Moreover, he found the "the critical velocity was very sensitive to disturbances in the water before entering the tubes". For large disturbances at the pipe inlet, the flow became unstable at lower critical velocities and at the critical velocity he noted that disturbances could appear intermittently for short distances, like "flashes", along the pipe. These "flashes" are today called turbulent spots or turbulent bursts.

#### 2.2. Classical linear stability theory

Lord Rayleigh [56](1880) started his theoretical investigations of the stability of parallel flow of an inviscid fluid at about the same time as Reynolds carried out his experiments with pipe flows. He explored the stability of disturbances linearised around the mean velocity profile  $\mathbf{U} = U(y)\overline{\mathbf{e}}_x$ , where x denotes the mean flow direction and y the direction normal to to the mean flow. By rewriting the linearised equations as an equation for the normal velocity component, v, and applying the following normal-mode assumption

$$v(x, y, t) = \text{Real}\{\hat{v}(y)e^{i\alpha(x-ct)}\},$$

where  $\alpha$  is the wave number, c is the complex wave velocity and t denotes time, he obtains the following stability equation

$$(U - c)(\frac{d^2}{du^2} - \alpha^2)\hat{v} - U''\hat{v} = 0, \tag{1}$$

governing the complex amplitude function,  $\hat{v}$ , of the normal velocity component. From this equation Rayleigh proved his inflection point theorem, stating that a necessary requirement for inviscid instability is that the mean velocity profile has an inflection point. Later Fjørtoft [20](1950) sharpened the requirement by proving it necessary for instability that

$$U''(U-U_s)<0,$$

somewhere in the flow, where  $U_s=U(y_s)$  is the mean velocity at the inflexion point, that is  $U''(y_s)=0$ . Note that both these theorems constitute necessary but not sufficient requirements for the inviscid flow to become unstable. Furthermore, it should be noted that the transition observed in pipe flow can not be explained by Rayleigh's inflection point theorem as the mean profile is not inflectional.

Rayleigh's work was followed by Orr [54](1907) and Sommerfeld [68](1908) who independently derived an equation in which effects of viscosity was included

$$(U - c)(\frac{d^2}{dy^2} - \alpha^2)\hat{v} - U''\hat{v} = \frac{1}{i\alpha Re}(\frac{d^2}{dy^2} - \alpha^2)^2\hat{v}.$$
 (2)

Heisenberg [27](1924) was the first to show that an inviscidly stable flow could become unstable for finite Reynolds numbers. He considered a plane Poiseuille flow using, asymptotic theory for large Reynolds numbers and small streamwise wave numbers, and became the first to find a solution to the Orr–Sommerfeld equations. From his rough calculations he estimated the critical Reynolds number to be around 1000.

The first useful solutions were worked out by members of Prandtl's group in Göttingen, by Tietjens [70](1925) and later Tollmien [71](1929) and Schlichting [61, 62](1933,1935). The last two developed a comprehensive theory for solving the Orr–Sommerfeld equations; hence today two-dimensional exponentially growing waves are named Tollmien–Schlichting (TS) waves. Lin [47](1944) developed the asymptotic theory further, and solved the Orr–Sommerfeld equations for plane Poiseuille flow estimating the critical Reynolds number to 5300. Today, computers allow for accurate numerical solutions to the Orr–Sommerfeld equations and Orszag [55](1971) showed that the critical Reynolds number for plane Poiseuille flow is 5772.

The existence of Tollmien–Schlichting waves was long questioned and it was not until the forties that the linear stability theory could be experimentally verified in all its essential details. During the second world war Schubauer & Skramstad [64](1947) (published later due to the war) conducted experiments on a flat plate using a vibrating ribbon to trigger the Tollmien–Schlichting waves and a hot-wire anemometry to measure the fluctuating streamwise velocity.

Tollmien—Schlichting waves in a plane Poiseuille flow proved even harder to verify experimentally. However, Nishioka *et al.* [53](1975) used similar methods as used in the flat plate boundary layer case and confirmed the theoretical results obtained by Orszag.

#### 2.3. Squire's theorem and the role of three-dimensionality

Squire [69](1933) made an important contribution to linear stability theory when he discovered that two-dimensional waves are the first to become unstable, and that an oblique wave always can be transformed into a two-dimensional wave associated with a lower critical Reynolds number, using the today well-known "Squire's theorem".

This threw a smoke-screen over the important role of three-dimensionality, and had the rather counter-productive effect that most of the early work on stability concerned only two-dimensional waves.

However, a decade later after Schubauer and Skramstad's verification of the Tollmien–Schlichting waves, when Emmons [18](1951) accidently noticed sporadic turbulent spots on shallow running water, two-dimensionality was nearly abandoned and soon, "everybody was seeing spots" as Morkovin [52](1969) wryly notes.

Today its common knowledge that three-dimensionality deserves attention for two main reasons. First, the later stages of transition caused by two-dimensional TS waves are highly three-dimensional. Second, there is strong evidence that subcritical disturbance growth is caused by three-dimensional disturbances.

# Spatially evolving disturbances and non-parallel effects

#### 3.1. Spatial stability and non-parallel effects

In section 2.2 the linear stability equations were discussed in terms of a temporal problem. The assumption of a real streamwise wave number,  $\alpha$ , but a complex wave velocity, c, implies a growth (or decay) of the wave disturbances with time. However, if instead the streamwise wavenumber is assumed complex while the frequency,  $\omega$ , is taken as a real number, these equations also governs the evolution of disturbances in space. Especially the physical situation for boundary layer flows often requires the modelling of disturbance quantities utilising the spatial approach. For example, the downstream development of an upstreamintroduced disturbance in a flat plate boundary layer flow is most appropriately modelled using the spatial framework. Since the spatial stability problem is given by an eigenvalue problem where the eigenvalue appears nonlinearly (up to the power of four), it is mathematically slightly more complicated than the temporal linear eigenproblem.

A further complication for boundary layer flows is caused by their *non-parallel* character. In contrast to the *parallel* channel and pipe flows the boundary layer base flows are dependent on the streamwise coordinate. Different perturbation approaches have been tried to incorporate non-parallel effects mathematically, but their validity is restricted to cases where the base flow divergence is slow compared to the spatial change of the disturbance quantities.

The effects of growing boundary layers have been introduced into the stability theory by several authors, e.g. Gaster [22], Saric & Nayfeh [60], Gaponov [21] and El-Hady [15].

#### 3.2. The Parabolised Stability Equations

Recently, a non-parallel stability theory based on parabolised stability equations (PSE) has been developed. The first to solve parabolic evolution equations for disturbances in the boundary layer was Hall [25], who considered steady Görtler vortices. Itoh [35] used a parabolic equation to study the evolution of small-amplitude Tollmien–Schlichting waves. The method was further developed by Herbert and Bertolotti [11, 32, 10, 12], who also derived the nonlinear

parabolised stability equations. Simen and Dallmann [65, 66] independently developed a similar theory. A review of the PSE-method and its potential for applications to a wide series of different flow-cases is given by Herbert [33].

The use of parabolised stability equations can be justified if the properties of the flow are slowly changing in the streamwise direction compared to the wall-normal direction. The first step in the derivation of the parabolised stability equations is separating the disturbances ( $\mathbf{q} = (u, v, p)^T$ ) into an amplitude function and an exponential function

$$\mathbf{q}(x, y, t) = \tilde{\mathbf{q}}(x, y) e^{i \int_{x_0}^x \alpha(\xi) d\xi - i\omega t},$$
(3)

where  $\alpha$  is the complex streamwise wavenumber (with the real and imaginary parts denoted  $\alpha_r$  and  $\alpha_i$ , respectively) and  $\omega$  the angular frequency. Introducing the above ansatz into the Navier–Stokes equations and making use of the assumption of slowly streamwise varying flow quantities, the amplitude functions,  $\tilde{u}, \tilde{v}$  and  $\tilde{p}$ , and the wavenumber,  $\alpha$ , are all assumed to be slowly varying functions of x. Thus

$$\frac{\partial}{\partial x}$$
,  $V \sim O(Re^{-1})$ ,

while the sizes of other quantities are assumed to be of O(1). Neglecting all terms of order  $O(Re^{-2})$  and higher, we arrive at a system of equations of the form

$$\tilde{\mathbf{q}}_x = \mathcal{L}\tilde{\mathbf{q}},\tag{4}$$

where  $\mathcal{L}$  contains wall-normal but no streamwise derivatives and where therefore no second-order x-derivatives are left in the now parabolised equations.

Since (4) represent a system of three equations governing four unknown quantities, a forth relation is needed for closure. The ambiguity stems from expression (3), where both the amplitude functions and the streamwise wavenumber are assumed to be functions of x, and no specification of there relationship is provided. The PSE provides this information via an additional equation, called the normalisation condition

$$\int_{y_{\min}}^{y_{\max}} (\tilde{u}^* \tilde{u}_x + \tilde{v}^* \tilde{v}_x + \tilde{p}^* \tilde{p}_x) \mathrm{d}y = 0, \tag{5}$$

where \* denotes complex conjugate. Other types of normalisation conditions can also be used. These relations all share the common characteristic to ensure that most of the disturbances x-variation will find its way into the exponential function. Thereby the streamwise variation of the amplitude function,  $\tilde{\mathbf{q}}$ , remains small, in accordance with the original assumption. Equations (4) are solved by marching downstream, starting with an appropriate initial condition, and ensuring that (5) is satisfied at each streamwise position.

The measurement of the streamwise change of  $\tilde{u}_{\text{max}}$  is an often used quantity in experiments as indicator for the growth of the disturbance. The chain rule

yields the expression

$$-\alpha_i + \text{Real}\left\{\frac{1}{\tilde{u}_{\text{max}}} \frac{\partial \tilde{u}_{\text{max}}}{\partial x}\right\},\tag{6}$$

for the corresponding growth rate extracted from the PSE-solution. Here  $\tilde{u}_{\max}$  denotes the maximum of  $\tilde{u}$  over the wall-normal coordinate, y.

An analysis of the parabolic stability equations reveal that there is still a weak ellipticity left in the equations, see Haj-Hariri [24]. As a consequence the use of an explicit scheme in the streamwise direction will produce numerical instabilities, and a crucial part of the PSE method is to use an implicit scheme with a large enough step-size in the streamwise direction. This critical step size was quantified by Li & Malik [44, 45] as

$$\Delta x > \frac{1}{|\alpha_r|},\tag{7}$$

and has proven correct for most of the PSE applications. More detailed information of the PSE approximation can be obtained by comparing fundamental solutions of the spatially formulated linearised two-dimensional Navier—Stokes equations and the PSEs with constant coefficients. Such a comparison shows that the parabolising procedure eliminates the most dangerous upstream propagating eigenmode and the remaining ellipticity makes the PSEs ill-posed as an initial-value problem in x, see Kreiss & Lorenz [41].

As presented in paper 1 in this thesis Andersson, Henningson & Hanifi [7] suggested a modification of the PSEs which make the equations well-posed and eliminate the step size restriction. This is done by approximating the streamwise derivative by a first order implicit (backward Euler) scheme and including a term proportional to a part of the leading truncation error,

$$\tau = \frac{\Delta x}{2} \tilde{\mathbf{q}}_{xx} = \frac{\Delta x}{2} (\mathcal{L}_x \tilde{\mathbf{q}} + \mathcal{L} \tilde{\mathbf{q}}_x) \approx \frac{\Delta x}{2} \mathcal{L} \tilde{\mathbf{q}}_x. \tag{8}$$

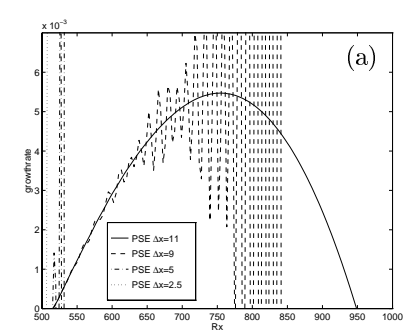
Here, the term  $\mathcal{L}_x\tilde{\mathbf{q}}$  has been neglected for simplicity. The assumption of small x-derivative terms implies that the added truncation error is of the order  $O(R^{-2})$ . Since terms of this order were neglected in the original approximation, the addition of  $\tau$  does not introduce any extra error at this order of approximation, and we can introduce the new set of equations

$$\tilde{\mathbf{q}}_x = \mathcal{L}\tilde{\mathbf{q}} + s\mathcal{L}\tilde{\mathbf{q}}_x,\tag{9}$$

where s is a positive real number. Based on the discussion given above, the differences between the solution of equations (4) and (9) are of order  $O(R^{-2})$ . Note that, although s take the place of  $\Delta x$  in the added truncation error term, this term is small, even if s = O(1), since  $\mathcal{L}\tilde{\mathbf{q}}_x$  is of order  $O(R^{-2})$ .

Andersson, Henningson & Hanifi [7] found the critical step size, for solving equation (9), with the first order backward Euler scheme, to be

$$\Delta x > \frac{1}{|\alpha_r|} - 2s. \tag{10}$$



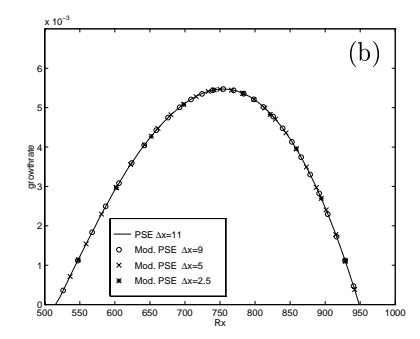


FIGURE 3.1 Growth rate vs streamwise position, for boundary-layer flow, obtained from the PSE method without (a) with (b) stabilising terms for the three smallest step sizes. The value of the stabilising parameter was set to s=4.

Equation (10) implies that the value of s giving marginal stability approaches  $0.5/|\alpha_r|$  when  $\Delta x \to 0$ . Consequently, this procedure makes it possible to stably march the PSEs downstream for any arbitrarily small step size by using a suitable s.

The stabilising procedure has been successfully applied to a number of flows, for example non-parallel boundary-layer flows. The equations were linearised around the two-dimensional Blasius boundary-layer flow. The calculations where performed with a disturbance frequency  $F = 70 \times 10^{-6}$ , where

$$F = \frac{2\pi\nu}{U_{\infty}^2} f,$$

with f being the physical frequency. The calculations were started at  $R=U_{\infty}\delta/\nu=500$ , where  $\delta=\sqrt{\nu L/U_{\infty}}$  and L the distance from the leading edge of the flat plate. The real part of the streamwise wavenumber was  $\alpha_r\approx 0.106$ , which gave a critical step size of approximately  $\Delta x=9.5$  based on the length scale at R=500.

Calculations of the growth rate were performed for four different step sizes  $\Delta x = 11$ , 9, 5 and 2.5. The growth rate was based on the maximum of  $\tilde{u}$  and evaluated using expression (6). In figure 3.1(a) the results for the original PSEs are presented. As can be seen a smooth solution were only obtained for the stable step size,  $\Delta x = 11$ . All attempts to march with step sizes under the critical value became numerically unstable at some point in the calculation domain.

The results from the modified PSEs with s=4 are given in figure 3.1(b). The disturbance growth rate calculated from the original PSEs for  $\Delta x=11$  is also given for reference purposes. As is shown there, numerical instability was absent in these calculations and results for all step sizes collapsed to the same curve.

## Non-modal amplification

#### 4.1. Lift-up and transient growth

Linear stability theory calculations of circular pipe flow reveal that all eigenvalues are stable and thus the flow is predicted to be stable. Even so, Reynolds reported transition to occur for high enough Reynolds numbers. Furthermore, both in plane Poiseuille flow and boundary flow, transition occur below the critical Reynolds number (subcritical transition) if the initial disturbance amplitudes are large enough. Clearly, another alternative growth mechanism to the one offered by classical linear stability theory is needed. Such a mechanism emerged during the 1980s and 1990s under the names of lift-up and transient or algebraic growth.

Landahl [42, 43] offered the physical explanation that a wall-normal displacement of a fluid element in a shear layer yields a large perturbation in streamwise velocity component, if the fluid element initially retains its horizontal momentum. An energy-efficient wall-normal redistributor of streamwise momentum consist of streamwise aligned vortices. It was therefore soon realised that a longitudinal externally generated vortex would "lift-up" low-velocity fluid on one side and push down high-velocity fluid on the other, creating the streak-like spanwise non-uniformity oriented in the streamwise direction that was observed in the flow visualisations.

Also Ellingsen & Palm [16] studied the lift-up effect and showed, within the inviscid approximation and provided a flow field without streamwise variation, that the streamwise velocity component could grow linearly with time. However, as explained by Hultgren & Gustavsson [34] in the presence of viscosity an initially inviscid "transient growth" will be followed by a viscous decay.

The development of an arbitrary linear three-dimensional disturbance superimposed on a laminar parallel base flow is governed by two equations. Besides the equation for the wall-normal velocity, v, an equation for wall-normal verticity  $(\eta = \partial u/\partial z - \partial w/\partial x)$  is needed

$$\left[\left(\frac{\partial}{\partial t} + U \frac{\partial}{\partial x}\right)\nabla^2 - U'' \frac{\partial}{\partial x} - \frac{1}{Re}\nabla^4\right]v = 0,\tag{11}$$

$$\left[\left(\frac{\partial}{\partial t} + U \frac{\partial}{\partial x}\right) - \frac{1}{Re} \nabla^2\right] \eta = -U' \frac{\partial v}{\partial z}.$$
 (12)

Here  $\nabla$  denote the nabla operator. If the normal-mode ansatz is introduced in the equations (11) and (12), the Orr–Sommerfeld equation (2) together with an equation denoted the Squire equation are obtained.

In classical linear stability theory only the least stable mode to the Orr–Sommerfeld equation (11) (TS wave) is considered. If this mode is damped, the flow is considered stable. However, the transient growth originates from the fact that the linear operator representing the coupled Orr–Sommerfeld and Squire equations (i.e. representing the evolution of an arbitrary three-dimensional disturbance) is non-normal and consequently have non-orthogonal eigenfunctions. This implicates that the total sum of modes, which individually are stable and consequently each will have amplitudes that decrease with time, can experience a strong transient growth phase before a viscous decay forces the disturbances to approach zero.

It is a well-established fact that the differential equations (11) and (12) governing an arbitrary three-dimensional disturbance are non-normal. Even so, the common notion in the transition community seems to have been that they should behave nearly as if they were. The non-coincidence of left and right eigenfunctions was for long viewed as a mere technicality. However, in recent years, governed by the idea of the lift-up phenomenon, researches such as Henningson, Lundbladh & Johansson [29] have gathered evidence to point upon a transient phase of algebraic growth that can sometimes be strong enough to bypass the exponential phase totally, making it unobservable in practice.

L. N. Trefethen introduced the notion of pseudospectra to quantify the non-normality of operators. This notion has been used by Trefethen *et al.* [72] to show that the departure from normality is indeed large in many flows.

#### 4.2. Optimal disturbances

**4.2.1.** Temporal setting. As we have seen and also as the title "non-modal amplification" suggests, the the instability caused by an arbitrary three-dimensional disturbance is not described by a single eigenmode (as is the case using the least stable TS wave to determine the stability), but rather by a sum of eigenmodes to equations (11) and (12). This results in a disturbance that changes its shape as each individual mode grow or decay with time, opposed to the expontially growing instability modes of constant form.

When considering disturbances of different shape, the natural question arises; which initial shape (given say unit energy) causes the maximum energy growth within a specified time period? Such disturbances are denoted *optimal perturbations* and were first studied in parallel shear flows by Farrell [19], Butler & Farrell [13] and Reddy & Henningson [57]. These studies found that disturbances which resemble streamwise vortices exhibit the strongest transient growth.

Gustavsson [23] studied transient growth in a Poiseuille flow before any optimal perturbations had been calculated. He used various Orr–Sommerfeld modes

together with zero normal vorticity as initial conditions and studied the response in the normal vorticity as a function of time. When triggering modes with zero streamwise wave number he obtained a maximum energy growth only slightly smaller than the one calculated for the optimal perturbation. A number of later studies have shown that weak streamwise vortices can trigger large streamwise velocity perturbations due to lift-up, and that in fact this mechanism can give rise to a transient growth phase strong enough to lead to transition.

4.2.2. Spatial setting. Recently, optimal disturbances and transient growth inside flat plate boundary layers have been studied using spatial settings. Andersson, Berggren & Henningson [4] and Luchini [49] used two slightly different formulations to study the linear stability of a high-Reynolds-number flow of a viscous, incompressible fluid over a flat plate (the geometry of the problem is shown in figure 1.1).

The objective for paper 2 in this thesis was to model disturbances that occur at moderate and high levels of free-stream turbulence. These disturbances are known to be elongated in the streamwise direction, to appear with a fairly spanwise periodic regularity and to vary on a slow timescale [75]. This motivates the use of boundary-layer approximations to the steady, incompressible Navier–Stokes equations, that is the Görtler equations, with the Görtler number set to zero. These equations are linearised around a two-dimensional Blasius base flow in order to obtain equations for the spatial evolution of three-dimensional disturbances. Due to the experimentally observed spanwise regularity the z-dependence is taken to be periodic, with the spanwise wavenumber denoted  $\beta$ .

The obtained stability equations are parabolic in x for the three velocity components, so that, given an initial velocity disturbance, as initial condition at a given  $x_0 > 0$ , we may solve the initial-boundary-value problem for  $x > x_0$  to obtain the downstream development of the given initial disturbance.

Luchini [48] simplified these equations further by considering the limit of small spanwise wavenumbers. In this limit the three-dimensional boundary layer equations were found to contain similarity solutions—consisting of eigensolutions—corresponding to a three-dimensional extension of the two-dimensional solutions studied by Libby & Fox [46]. The approximation becomes invalid when the spanwise wave length is of the order of the boundary layer thickness. However, within the approximation, a least stable mode is found that allows for an algebraic growth of the streamwise velocity in the streamwise direction according to  $u \sim x^{0.21}$ .

The mathematical problem of finding the optimal disturbances, can be formulated using a notation in abstract operators. We adopt an input-output point of view and consider the 'output'

$$\mathbf{u}_{\text{out}} = (u(x, y), \ v(x, y), \ w(x, y))^T \tag{13}$$

at  $x > x_0$  as given by the solution of the parabolic initial-boundary-value problem discussed above with the 'input' data

$$\mathbf{u}_{\rm in} = (u_0(y), \ v_0(y), \ w_0(y))^T. \tag{14}$$

Since the problem is linear and homogeneous, we may write this

$$\mathbf{u}_{\text{out}} = A\mathbf{u}_{\text{in}} \tag{15}$$

where A is a linear operator.

The downstream development of disturbances is studied by observing how the output  $\mathbf{u}_{\text{out}}$  changes with the input  $\mathbf{u}_{\text{in}}$ . To quantify the 'size' of these disturbances we define a measure of the disturbance energy at a specific streamwise location x,

$$E(\mathbf{u}(x)) = \int_0^\infty (Re |u|^2 + |v|^2 + |w|^2) \, dy \equiv ||\mathbf{u}||^2 = (\mathbf{u}, \mathbf{u}), \tag{16}$$

where  $|\cdot|$  denotes the absolute value and where Re is the Reynolds number based on the streamwise distance to the leading edge of the flat plate. The appearance of Re in the norm is a result of the boundary-layer scaling and ensures that the physical velocity components have equal weight. Note that the square root of the disturbance energy is a norm, given by an inner product, on the space of disturbances at a fixed streamwise location.

To calculate the optimal disturbance, we pick two streamwise locations  $0 < x_0 < x_f$  and maximise the output disturbance energy at  $x = x_f$  among all suitable constrained inputs at  $x = x_0$  with fixed (unit) energy. The maximised quantity is denoted the maximum spatial transient growth,

$$G(x_f) = \max_{E(\mathbf{u}_{\text{in}})=1} E(\mathbf{u}_{\text{out}}(x_f)) = \max_{\|\mathbf{u}_{\text{in}}\|=1} \|\mathbf{u}_{\text{out}}(x_f)\|^2 = \max_{\|\mathbf{u}_{\text{in}}\|=1} \|\mathcal{A}\mathbf{u}_{\text{in}}\|^2. \quad (17)$$

Expression (17) can be reformulated as

$$G(x_f) = \max_{\mathbf{u}_{\text{in}} \neq 0} \frac{\|\mathcal{A}\mathbf{u}_{\text{in}}\|^2}{\|\mathbf{u}_{\text{in}}\|^2} = \max_{\mathbf{u}_{\text{in}} \neq 0} \frac{(\mathcal{A}\mathbf{u}_{\text{in}}, \mathcal{A}\mathbf{u}_{\text{in}})}{(\mathbf{u}_{\text{in}}, \mathbf{u}_{\text{in}})} = \max_{\mathbf{u}_{\text{in}} \neq 0} \frac{(\mathbf{u}_{\text{in}}, \mathcal{A}^* \mathcal{A}\mathbf{u}_{\text{in}})}{(\mathbf{u}_{\text{in}}, \mathbf{u}_{\text{in}})}, \quad (18)$$

where the operator  $\mathcal{A}^*$  in equation (18) denote the adjoint operator to  $\mathcal{A}$  with respect to the chosen inner product. Recalling some basic facts from operator theory it can be noted that if the maximum of  $(\mathcal{A}\mathbf{u}_{in}, \mathcal{A}\mathbf{u}_{in})/(\mathbf{u}_{in}, \mathbf{u}_{in})$  is attained for some vector  $\overline{\mathbf{u}}_{in}$ , this vector is an eigenvector corresponding to the largest eigenvalue of the eigenproblem

$$A^*A\mathbf{u}_{\rm in} = \lambda \mathbf{u}_{\rm in},\tag{19}$$

and  $G(x_f)$  is the maximum eigenvalue, necessarily real and nonnegative.

The eigenvector corresponding to the largest eigenvalue of (19) can be calculated using *power iterations*,

$$\mathbf{u}_{\text{in}}^{n+1} = \rho^n \mathcal{A}^* \mathcal{A} \mathbf{u}_{\text{in}}^n, \tag{20}$$

where  $\rho_n$  is an arbitrary scaling parameter, used to scale the iterates to unit norm, for instance. If the largest eigenvalue,  $\lambda$ , is separated from the rest of the

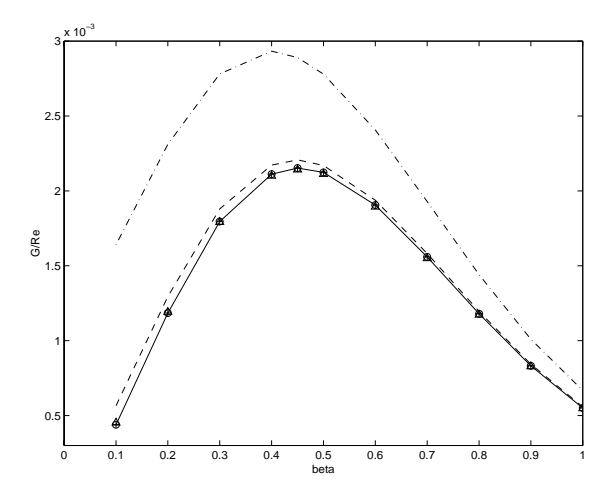
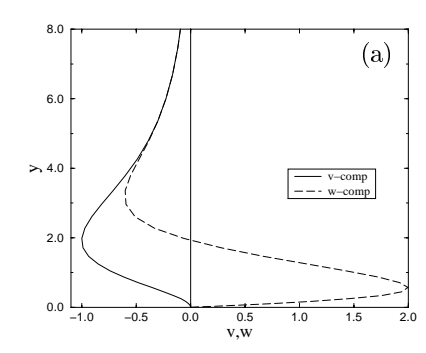


FIGURE 4.1 Maximum spatial transient growth divided by the Reynolds number versus spanwise wave number. Here  $x_0=0$  and  $x_f=1$ . (----  $Re=10^3$ , - - -  $Re=10^4$ ,  $\Delta$   $Re=10^5$ , +  $Re=10^6$ , o  $Re=10^9$ , — Re-independent)

spectrum, the power iterations converge so that  $\lim_{n\to\infty} \mathbf{u}_{\rm in}^n/||\mathbf{u}_{\rm in}^n|| = \overline{\mathbf{u}}_{\rm in}$ . From  $\overline{\mathbf{u}}_{\rm in}$  it is then possible to calculate  $\mathbf{u}_{\rm out}(x_f) = \mathcal{A}\overline{\mathbf{u}}_{\rm in}$  and the maximum energy growth,  $G(x_f)$ .

Starting from the leading edge  $(x_0 = 0)$ , the Görtler equations, with the Görtler number set to zero, are integrated a unit distance  $(x_f = 1)$  downstream, and G are calculated for several values of  $\beta$ . The calculations are repeated for five different Reynolds numbers  $Re = 10^3$ ,  $10^4$ ,  $10^5$ ,  $10^6$  and  $10^9$ , and once with a Reynolds-number-independent formulation used by Luchini [49]. Figure 4.1 depicts G(x)/Re versus  $\beta$  and shows that the maximum spatial transient growth scales linearly with the distance from the leading edge for large Reynolds numbers.

The v and w components of the optimal perturbation, for the spanwise wave number  $\beta=0.45$  and optimised with respect to downstream position x=1, are given in figure 4.2(a) at the high-Reynolds-number limit. The corresponding u component of the response at the downstream position x=1 caused by this optimal perturbation is given in figure 4.2(b). For high Reynolds numbers, the u component almost completely vanishes in the optimal perturbation compared with the v and w components. Likewise, the v and w components vanish in comparison with the u component in the downstream response. This is a consequence of the appearance of the Reynolds number Re in the disturbance energy (16). Note that, because of the periodicity property in the spanwise direction, the upstream disturbance in figure 4.2(a) corresponds to streamwise vortices and the downstream response in figure 4.2(b) to streamwise streaks. Also plotted in



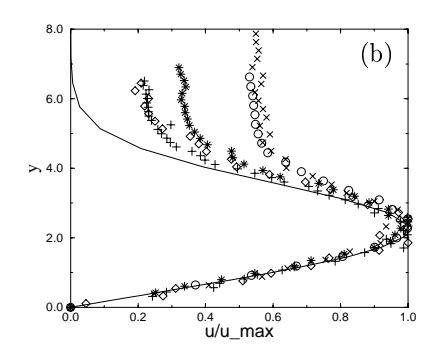
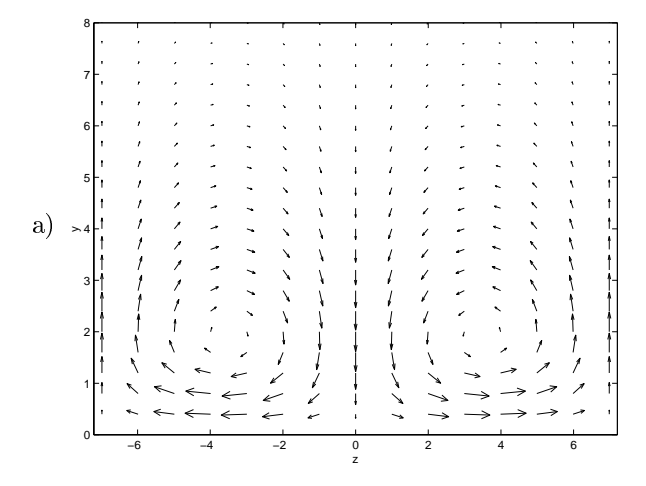


FIGURE 4.2 (a) The optimal perturbations at the leading edge maximised with respect to the downstream position x=1. Here  $\beta=0.45$ . The u component is zero. (b) Downstream response at x=1 corresponding to the optimal perturbations in the left figure, that is  $\beta=0.45$ . The v and w components are zero. Also a comparison with experimental data [75] measured in a flat-plate boundary layer at different downstream locations.

figure 4.2(b) are the experimental data from Westin et al. [75]. All the streamwise velocity components have been normalised to unit maximum value. The presence of free-stream turbulence in the experiments prevents the root-mean-square streamwise velocity perturbations to vanish at infinity. The remarkably good agreement between the measured and calculated velocity profiles, and the fact that the calculations contained an optimisation procedure while the experiments did not, indicate that the shown profile corresponds to some dominating, fundamental mode triggered in the flat plate boundary layer when subjected to high enough levels of free-stream turbulence. The fact that the power iterations converges quickly, also indicates the existence of a well-separated, dominating mode. The main conclusion is that almost any steady initial disturbance will develop into a streamwise streak given a large enough Reynolds number. A more complete version of the above material is given in Andersson et al. [4].

Figures 4.3 further visualise the upstream disturbance and the corresponding downstream response, as given in figures 4.2(a) and 4.2(b). In figure 4.3(a) we give the upstream disturbance plotted as velocity vectors in the z-y plane. The corresponding downstream response is shown as contours of constant streamwise velocity in the z-y plane in figure 4.3(b). Note how the low velocity streaks are produced by the lift-up of low velocity fluid elements near the wall and correspondingly how the high velocity streaks are produced by the introduction of high velocity fluid elements pulled down from the free-stream.

The simplified model proposed by Luchini [48] allows for a self-similar solution consisting of eigenmodes. One can show that the corresponding eigenvalues are all positive and real, and that the eigenfunctions form a complete set. An



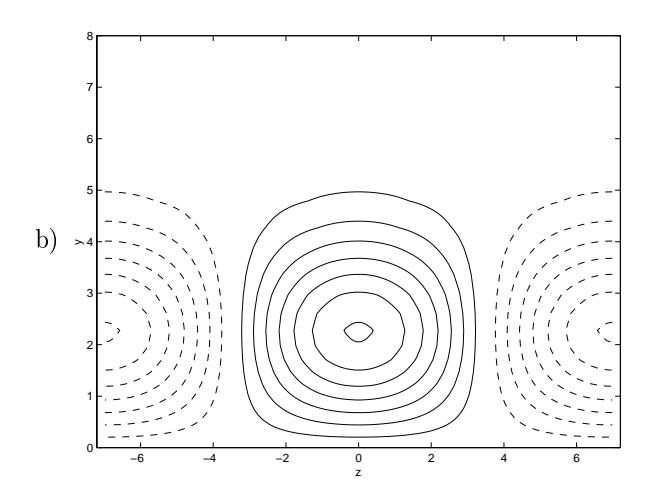


FIGURE 4.3 (a) Velocity vectors in the z-y plane of the optimal disturbance at  $x=x_0$ . Here  $x_0=0$  and  $\beta=0.45$ . The u component is zero. (b) Contours of constant streamwise velocity representing the downstream response at  $x=x_f=1$  corresponding to the optimal disturbance shown in the above figure. The v and w components are zero. Here, solid lines represent positive values and dashed lines represent negative values.

arbitrary disturbance can therefore be expanded in a sum of modes. Schmid [63] used these modal solutions to optimise the total disturbance energy gain between two streamwise locations, by superimposing a number of modal solutions. By using a projection of the flow onto the space spanned by the eigenvectors, the disturbance energy density is given in a quadratic form. He then formulated the optimisation problem using a variational form, where a Lagrange multiplier is used to enforce initial conditions of unit energy. When solving the resulting Euler-Lagrange equations, in form of a generalised eigenvalue problem, he finds that a substantial gain in energy can be achieved before the asymptotic behaviour (given by the unstable mode) dominates the growth in energy.

This asymptotic behaviour corresponds to the mode with the spatial algebraic growth of the streamwise velocity component of  $u \sim x^{0.21}$ . For distances sufficiently far downstream of the leading edge, where this mode prevails, the mode shape shows a similar velocity profile as that corresponding to the optimal streak displayed in figure 4.2(b), see paper 5 in this thesis (Andersson [3]).

There is, however, a fundamental difference in the prediction of the spatial growth of the streamwise velocity components between the two models. While the solution to the eigenproblem grows unboundedly with the streamwise coordinate as  $x^{0.21}$ ; the streamwise streaks from the more general model, determined by the optimisation calculations, will always obtain a maximum at a given streamwise position and vanish as  $x \to \infty$ . This difference in behaviour is a result of having retained the spanwise diffusive term  $-\beta^2 \mathbf{u}$  in the more general model.

## Secondary instability

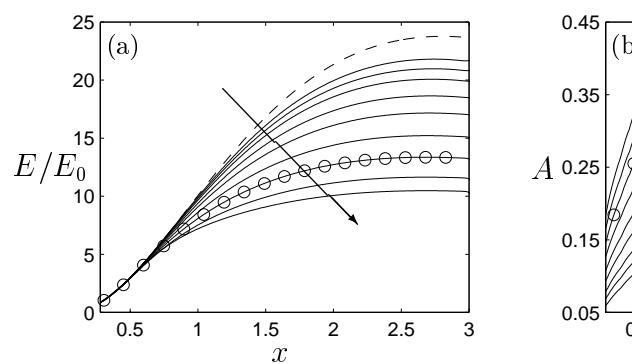
#### 5.1. Saturation and general introduction of secondary instability

In the previous chapters the linear amplification of the small-amplitude disturbances were supplied by either of two different mechanisms; the two-dimensional waves in chapters 2 and 3 or the growth of streaks in chapter 4. These type of disturbances will here be denoted *primary instabilities*. If the amplification is strong enough the disturbances eventually reach an amplitude where nonlinear effects become important. A possible but very unusual scenario is that the primary instability transforms the flow directly into a turbulent state. More likely the disturbances saturate and take the flow into a new steady or quasi-steady state.

The spatial development of such a quasi-steady state is displayed in figures 5.1. The nonlinear development of the optimal streaks discussed in section 4.2.2 are computed solving the full Navier–Stokes equations in a spatially evolving boundary layer. Details on the solution procedure, using direct numerical simulations, can be found in Andersson et al. [6] (paper 3 in this thesis). The complete velocity field from the linear results by Andersson, Berggren & Henningson [4] is used as input close to the leading edge and the downstream nonlinear development is monitored for different initial amplitudes of the perturbation. This is shown in figure 5.1(a), where all energies are normalised by their initial values. The dashed line corresponds to an initial energy small enough for the disturbance to obey the linearised equations. Figure 5.1(b) displays the downstream amplitude development for the same initial conditions as figure 5.1(a).

This new saturated flow—that is the base flow plus the primary instability—may itself become unstable to perturbations different from those which grow in the presence of the base flow alone; such instabilities are usually denoted secondary instabilities. The secondary instability stage often occurs on a much faster timescale than the primary instability, making a steady-state assumption reasonable even in cases with a quasi-steady flow state.

Here, three different scenarios in a flat plate boundary layer flow are considered; secondary instability of two-dimensional waves, secondary instability of streaks and a brief description of oblique transition.



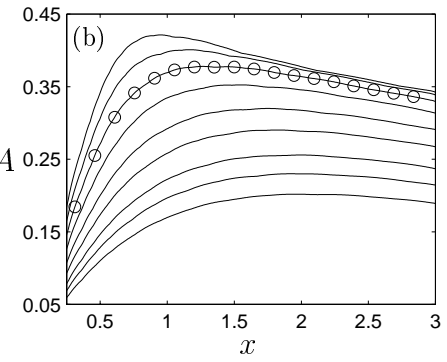
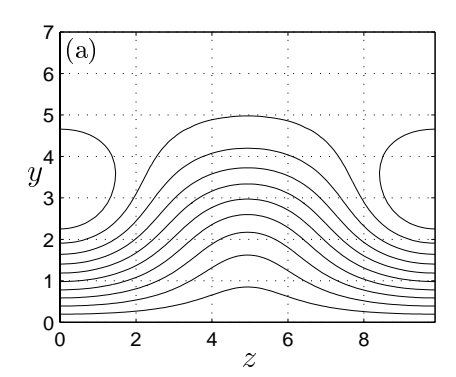


FIGURE 5.1 (a) The energy, as defined in (16), of the primary disturbance, E, normalised with its initial value,  $E_0$ , versus the streamwise coordinate, x, for  $\beta$ =0.45 and  $Re_{\delta}$ =430. Here x has been made non-dimensional using the distance to the leading edge. The arrow points in the direction of increasing initial energies. The dashed line represents the optimal linear growth. (b) The downstream amplitude development for the same initial conditions as in (a). The amplitude A is defined by equation (22). (The two lines have been circled for future reference).

#### 5.2. Secondary instability of two-dimensional waves

If the amplitude of an amplified Tollmien-Schlichting wave grow above a given threshold it becomes susceptible to secondary instabilities. Experimental investigators identified two possible three-dimensional stages between the twodimensional state and fully developed turbulence. One of these two types of secondary instabilities was observed by Klebanoff, Tidstrom & Sargent [39] and was later denoted K-type after Klebanoff but is also called fundamental breakdown since the frequency of the secondary instability is the same as that of the primary instability. This transition scenario gives rise to a structure consisting of  $\Lambda$ -shaped vortices aligned in the streamwise direction and has been observed in flow visualisation studies. The other transition scenario also shows  $\Lambda$ -shaped vortices but in this case the structures are arranged in a staggered pattern which suggests a secondary instability with half the frequency of the one associated with the primary wave and is thus often denoted subharmonic breakdown. This type of secondary instability is also denoted H-type after the theoretical work by Herbert [30, 31] or N-type after "Novosibirsk" where the group Kachanov, Kozlov & Levchenko [38] first observed this scenario in experimental studies. Transition experiments with controlled two-dimensional Tollmien-Schlichting waves reveal that the subharmonic secondary instability is the first to appear when smallamplitude forcing is used, whereas for larger initial amplitudes, the fundamental secondary instability type is usually observed. Consequently, in low ambient



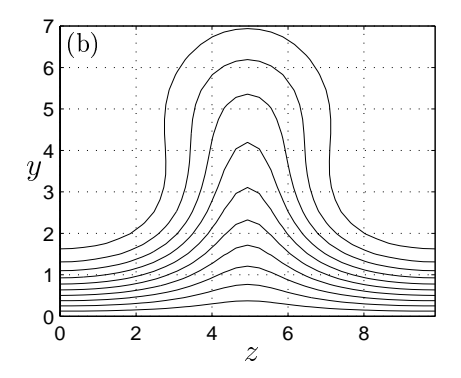


FIGURE 5.2 Contour plots in a z-y plane of the primary disturbance streamwise velocity using the spanwise wavenumber  $\beta = 0.45$  and the disturbance amplitude A = 0.36 at the streamwise position x = 2 for (a) the shape assumption; (b) the nonlinear mean field corresponding to the circled line in figures 5.1 at x = 2 (where A = 0.36). Here  $Re_{\delta} = 430$ . In both figures the coordinates y and z have been made non-dimensional using the local Blasius length scale  $\delta$ , at streamwise position x = 2.

disturbance environments the subharmonic secondary instability is more likely to occur inside boundary layers. For a review over the theoretical aspects and the physical mechanisms involved to explain the secondary instabilities, see Herbert [31] and Kachanov [37]. The investigations of the different types of breakdown scenarios performed using direct numerical simulations have been reviewed by Kleiser & Zang [40].

#### 5.3. Secondary instability of streaks

If the disturbance energy of the streaks becomes sufficiently large, secondary instability can take place and provoke early breakdown and transition, overruling the theoretically predicted modal decay. A possible secondary instability is caused by inflectional profiles of the base flow velocity, a mechanism which does not rely on the presence of viscosity. Experiments with flow visualisations by for example Alfredsson & Matsubara [2] have considered the case of transition induced by streaks formed by the passage of the fluid through the screens of the wind-tunnel settling chamber. They report on the presence of a high frequency "wiggle" of the streak with a subsequent breakdown into a turbulent spot.

In paper 3 in this thesis this secondary instability is studied using equations linearised around a mean field consisting of the complete nonlinear development of the streak. These secondary stability calculations are carried out under the following two assumptions:

- 1. Since the base flow is computed on the basis of the boundary layer approximation, the mean field to leading order will consist only of the streamwise velocity component. Such a mean field varies on a slow streamwise scale.
- 2. The perturbation is assumed to vary rapidly along the streamwise direction in comparison to the mean field. This is clearly observed in the experimental visualisations of Alfredsson & Matsubara [2]. Hence, our leading order stability problem is the parallel flow problem, with perturbation mode shapes dependent only on the cross-stream coordinates.

Under these assumptions the streak velocity field can be written on the form  $\mathbf{U} = (U(y, z), 0, 0)$ . Since the velocity field is periodic in the spanwise direction it may be expanded in the sum of cosines

$$U(y,z) = U_0(y) + \sum_{k=1}^{\infty} U_k(y) \cos(k\beta z),$$
 (21)

where  $U_0$  differs from the Blasius solution  $U_B$  by the mean flow distortion term. To be able to quantify the size of the primary disturbance field an amplitude A is defined as

$$A = \frac{1}{2} \left[ \max_{y,z} (U - U_B) - \min_{y,z} (U - U_B) \right]. \tag{22}$$

The effect of the nonlinear interactions on the base flow are shown by the contour plots in figures 5.2. Figure 5.2(a) displays the primary disturbance obtained using the shape assumption—where the primary disturbance (the linearly obtained streak) has been superimposed on the laminar mean field (the Blasius solution)—with A=0.36, while 5.2(b) shows a fully nonlinear mean field, characterised by the same disturbance amplitude. In the latter case, the low speed region is narrower and displaced further away from the wall.

The equations governing the stability of the streak are obtained by substituting  $\mathbf{U}+\mathbf{u}$ , where  $\mathbf{u}(x,y,z,t)=(u,v,w)$  is the perturbation velocity and  $\mathbf{U}$  is the streak profile above, into the Navier–Stokes equations and dropping nonlinear terms in the perturbation. The resulting equations are

$$u_t + Uu_x + U_y v + U_z w = -p_x + \frac{1}{Re} \Delta u, \qquad (23)$$

$$v_t + Uv_x = -p_y + \frac{1}{Re}\Delta v, (24)$$

$$w_t + Uw_x = -p_z + \frac{1}{Re}\Delta w, (25)$$

$$u_x + v_y + w_z = 0. (26)$$

Here p = p(x, y, z, t) is the perturbation pressure. The above equations can be reduced to two equations by expressing the perturbation quantities in terms of the normal velocity v and the normal verticity  $\eta = u_z - w_x$ . The manipulations

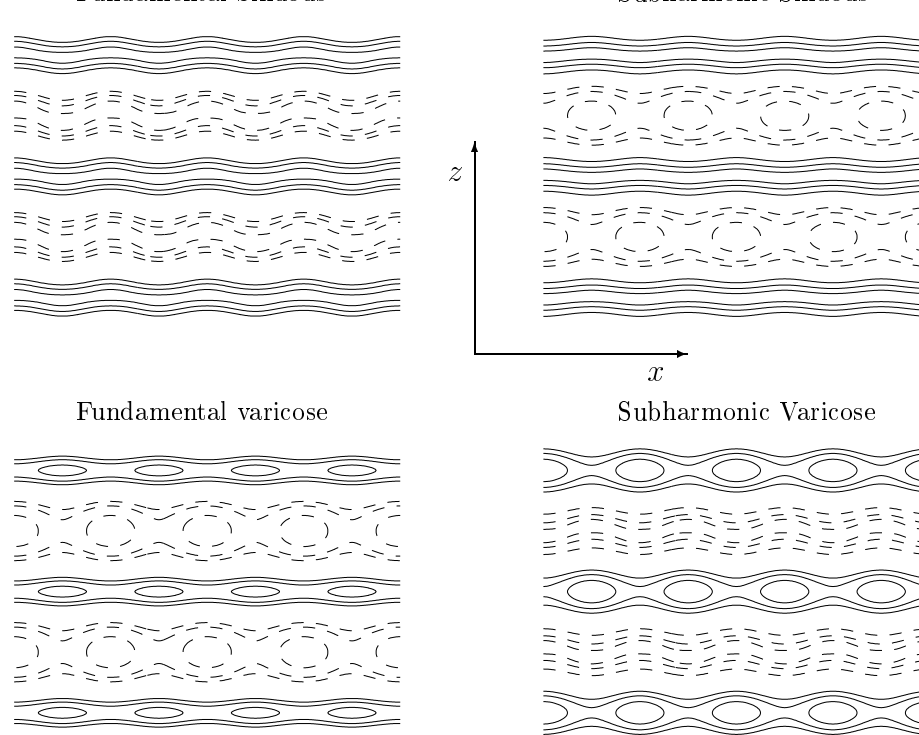


FIGURE 5.3 Sketch of streak instability modes in the x-z plane over four streamwise and two spanwise periods, by contours of the total streamwise velocity. The low-speed streaks are drawn with solid lines while dashed lines are used for the high-speed streaks.

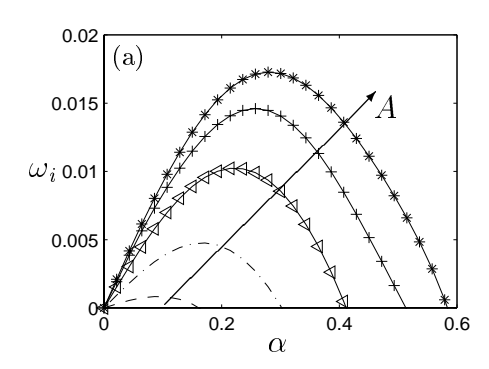
are similar to those in the derivation of the Orr–Sommerfeld and Squire equations showed earlier

$$\begin{split} \Delta v_t + U \Delta v_x + U_{zz} v_x + 2 U_z v_{xz} - U_{yy} v_x - 2 U_z w_{xy} - 2 U_{yz} w_x &= \frac{1}{Re} \Delta \Delta v, \\ \eta_t + U \eta_x - U_z v_y + U_{yz} v + U_y v_z + U_{zz} w &= \frac{1}{Re} \Delta \eta. \end{split}$$

Also the spanwise velocity w can be eliminated from the above equations using the identity

$$w_{xx} + w_{zz} = -\eta_x - v_{yz}.$$

Even if viscosity is neglected ( $Re \to \infty$  in equations (23)-(25)) the presence of both wall-normal and spanwise gradients in the mean field makes it impossible to obtain an uncoupled equation for either of the velocity components. It is, however, possible to find an uncoupled equation for the pressure by taking



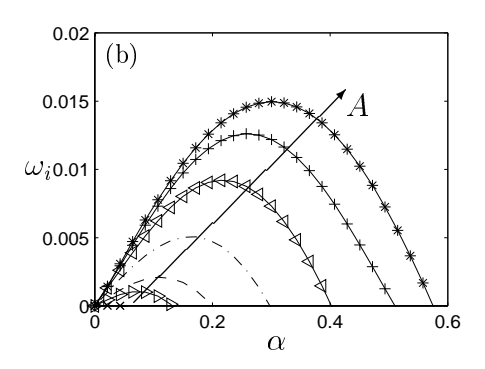


FIGURE 5.4 Temporal growth rates versus streamwise wavenumber for the (a) fundamental (b) subharmonic sinuous symmetries of the secondary instabilities; given for the different amplitudes of the primary disturbance ( $-\times A=25.6, -\triangleright-$  A=27.2, --- A=28.8, --- A=31.7, --- A=34.5, --+- A=36.4, --\*- A=37.3). The arrows point in the direction of increasing A's.

the divergence of the momentum equations, introducing continuity and then applying equations (24) and (25) (Henningson [28]; Hall & Horseman [26]). These manipulations yield

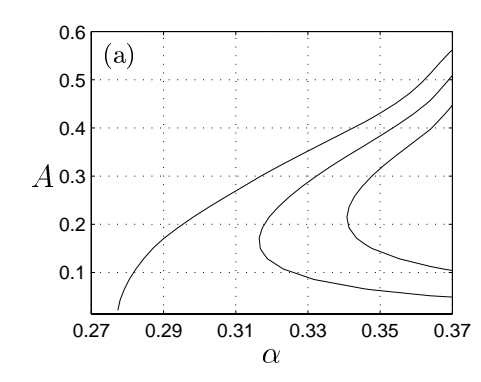
$$\left(\frac{\partial}{\partial t} + U\frac{\partial}{\partial x}\right)\Delta p - 2U_y p_{xy} - 2U_z p_{xz} = 0. \tag{27}$$

The pressure is expanded in an infinite sum of Fourier modes and only perturbation quantities consisting of a single wave component in the streamwise direction are considered, i.e.

$$p(x,y,z,t) = Real\{e^{i\alpha(x-ct)} \sum_{k=-\infty}^{\infty} \hat{p}_k(y)e^{i(k+\gamma)\beta z}\},$$

where  $\alpha$  is the real streamwise wavenumber and  $c=c_r+ic_i$  is the phase speed. Here  $\beta$  is the spanwise wavenumber of the primary disturbance field and  $\gamma$  is the (real) Floquet exponent. Because of symmetry it is sufficient to study values of  $\gamma$  between zero and one half, with  $\gamma=0$  corresponding to a fundamental instability mode, and  $\gamma=0.5$  corresponding to a subharmonic mode (see Herbert [31] for a thorough discussion on fundamental and detuned instability modes).

The most commonly used definitions of sinuous or varicose modes of instability are adopted with reference to the visual appearance of the motion of the low-speed streaks. A sketch of the different fundamental and subharmonic modes is provided in figure 5.3: it clearly illustrates how the symmetries of the subharmonic sinuous/varicose fluctuations of the low-speed streaks are always associated to staggered (in x) varicose/sinuous oscillations of the high-speed streaks.



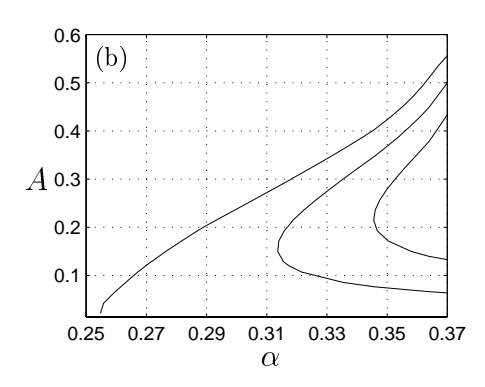


FIGURE 5.5 Neutral curves for streak instability in the A- $\alpha$  plane for (a) fundamental sinuous mode, (b) subharmonic sinuous mode. (contour levels:  $\omega_i$ =0, 0.0046, 0.0092)

In [6] (paper 3 of this thesis) an extensive parametric study was carried out for the sinuous fundamental ( $\gamma=0$ ), arbitrarily detuned ( $0<\gamma<0.5$ ) and subharmonic ( $\gamma=0.5$ ) symmetries, which were the only ones found to be significantly unstable. In figures 5.4(a) and 5.4(b) the growth rates of the instability  $\omega_i=\alpha c_i$  are plotted against the streamwise wavenumber, for the fundamental and subharmonic sinuous symmetries, respectively; and for different amplitudes of the streaks, obtained with the direct numerical simulations. One can note that when increasing the amplitude, not only do the growth rates increase but their maxima are also shifted towards larger values of the streamwise wavenumber  $\alpha$ . For amplitudes larger than about 0.30, the subharmonic symmetry produces lower maximum growth rates than the fundamental symmetry. Note, however, that for lower amplitudes the sinuous subharmonic symmetry represents the most unstable mode. The phase speeds for the two sinuous modes were found to be only weakly dispersive.

A study was also conducted in [6] to identify the neutral stability curves calculated for a range of  $\alpha$ 's. The results are displayed in figures 5.5 for the two sinuous symmetries, together with contour levels of constant growth rates. It can immediately be observed that a streak amplitude of about 26% of the free-stream speed is needed for an instability to occur. One can also notice that the subharmonic mode is unstable for lower amplitudes than the fundamental mode and that the growth rates for larger amplitudes are quite close for the two symmetries.

No results for the varicose instabilities are presented here. In fact, both the varicose fundamental and the subharmonic symmetries result in weak instabilities for amplitudes larger than  $A{=}0.37$  with growth rates smaller than one fifth of the corresponding sinuous growth rates. Therefore a breakdown scenario triggered by a varicose instability seems unlikely.

Andersson et al. [6] (paper 3 in this thesis) showed that the linear and non-linear spatial development of optimal streamwise streaks are both well described by the boundary layer approximations and as a consequence Reynolds number independent for large enough Reynolds numbers. This results in a boundary layer scaling property that couples the streamwise and spanwise scales, implying that the same solution is valid for every combination of x and  $\beta$  such that the product  $x\beta^2$  stays constant. The parameter study of streak's instability is therefore representative of a wide range of intermediate values of  $\beta$  for which saturation occurs at a reasonable x; large enough so that the boundary layer approximation may still be valid and small enough so that Tollmien–Schlichting waves may not play a significant role.

The secondary instability of streaks approximated by the *shape assumption* was parametrically studied by [5] (see paper 4 in this thesis). Comparison of the results with those obtained from calculations where the base flow is the nonlinearly developed streak demonstrate the inapplicability of the shape assumption for this type of studies. The secondary instability results are found to be very sensitive to a slight change in the shape of the mean field velocity profile and, even if the sinuous modes are reasonably well captured by the shape assumption, the growth rates of varicose modes are widely over-predicted.

#### 5.4. Oblique transition

In the last section the primary disturbance consisted of streamwise streaks and in chapter 4 it was shown how the initial disturbance optimally suitable for producing these streaks are streamwise aligned vortices. In the oblique transition scenario, streamwise aligned vortices are generated by nonlinear interaction between a pair of oblique waves with wave angles of equal magnitude but opposite sign. The oblique transition scenario is initiated by the oblique waves generating streamwise aligned vortices which, in turn, produces streamwise streaks. As the initial oblique waves start to decay the flow field becomes dominated by the streaky structures. If the amplitude of these streamwise streaks reaches above a threshold they become unstable to the same types of secondary instabilities as discussed in the previous section. The oblique transition scenario in a Blasius boundary layer has been studied experimentally by Wiegel [76] and Elofsson [17] and numerically by Joslin, Streett & Chang [36] and Berlin, Lundbladh & Henningson [8]. A comparison between Wiegels experiment and direct numerical simulations was presented by Berlin, Wiegel & Henningson [9].

#### CHAPTER 6

# Transition modelling for high free-stream turbulence levels

#### 6.1. "Classical" empirical correlations

Several empirical correlations for transition criteria involving the combined effects of the free-stream turbulence level and the streamwise pressure gradient have been developed. For example, van Driest & Blumer [73] arrives at a semi-empirical model, by introducing a critical vorticity Reynolds number that correlates the pressure gradient and free-stream turbulence level with the Reynolds number at transition. In the model of Dunham [14], the value of the Reynolds number based on momentum-loss thickness at the transition point is given as a function of the Pohlhausen (pressure gradient) parameter and the free-stream turbulence level. Abu-Ghannam & Shaw [1] suggest a model that gives the start and end of the transition region in terms of the Reynolds number based on momentum-loss thickness. Also here, the free-stream turbulence level and a pressure-gradient parameter are the only required inputs. For flows similar to the ones for which these empirical correlations are calibrated they often give reasonable predictions. However, the large degree of empiricism also implies that their generality is rather limited.

#### **6.2.** Model based on the $e^N$ -method

The  $e^N$ -method assumes that transition occurs when the most amplified exponentially growing disturbance has grown a factor  $N = \ln(A/A_0)$ , where  $A_0$  is the amplitude at the critical Reynolds number and A is the amplitude downstream. This growth is governed by linear stability theory. The prediction given by the  $e^N$ -method is that N is a constant or a function of the turbulence level in the free-stream. This method was developed independently by Smith & Gamberoni [67] and van Ingen [74]. Mack [50] used a modified  $e^N$ -method and suggested the empirical relationship,  $N = -8.43 - 2.4 \ln(\text{Tu})$ , between the free-stream turbulence level Tu and the N-factor at the transition location. This model gives reasonable transition locations in the range 0.1 < Tu < 2%.

Table 1 Comparisons of different experimental studies

	$\mathrm{Tu}(\%)$	$Re_T$	K
Roach & Brierley [59]			
T3AM	0.9	1,600,000	1138
T3A	3.0	$144,\!000$	1138
T3B	6.0	63,000	1506
Yang & Voke [77]	5.0	$51,\!200$	1131
Matsubara [51]			
$\operatorname{grid} A$	2.0	400,000	1265
grid B	1.5	1,000,000	1500

#### 6.3. Transition prediction based on non-modal amplification

Experimental measurements inside flat plate boundary layers indicate that for free-stream turbulence levels between roughly 1–5 %, transition is associated with growing streamwise streaks. In paper 2 in this thesis Andersson, Berggren & Henningson [4] propose a transition prediction model valid in this range based on the scaling property displayed in figure 4.1 together with three assumptions.

The first assumption is about the receptivity process at the leading edge of the flat plate. The input energy  $E(\mathbf{u}_{\rm in})$ , as defined in (16), is assumed to be proportional to the free-stream turbulence energy,

$$E(\mathbf{u}_{\rm in}) \propto \mathrm{Tu}^2.$$
 (28)

Second, we assume that the initial disturbance grows with the optimal rate,

$$E(\mathbf{u}_{\text{out}}) = GE(\mathbf{u}_{\text{in}}) = \overline{G} Re E(\mathbf{u}_{\text{in}}), \tag{29}$$

where  $\overline{G}$  is Reynolds-number independent. The last equality was found to hold for large enough Reynolds numbers (see figure 4.1 in section 4.2.2).

The third assumption is the existence of a threshold in the disturbance energy over which transition occurs. We assume that transition takes place when the output energy reaches the specific value,  $E_T$ ,

$$E(\mathbf{u}_{\text{out}}) = E_T. \tag{30}$$

Combining assumptions (28)–(30), we obtain

$$\sqrt{Re_T}$$
 Tu =  $K$ ,

where K should be constant for free-stream turbulence levels at 1–5 %. The experimental data used to verify this model are given in table 1. As can be seen, K is approximately constant for a variety of free-stream turbulence levels. A similar model, obtained from different arguments was given by van Driest & Blumer [73]. They postulated that transition occurs when the maximum vorticity Reynolds number reaches a critical value to be correlated with the free-stream turbulence level. A comparison between the two models and the experimental

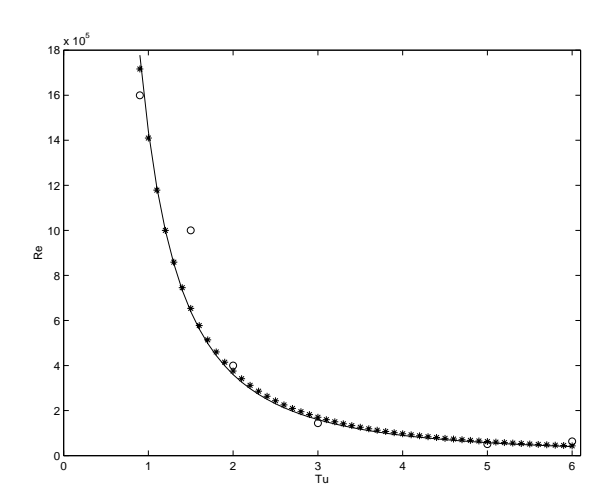


FIGURE 6.1 Transitional Reynolds number based on the distance to the leading edge versus free-stream turbulence level (given in percent), for two transition prediction models and experimental data. (— The model suggested in this paper with K=1200, \* The model proposed by van Driest & Blumer, o The experimental data from table 1.)

data given in table 1 is shown in figure 6.1. As can be seen there their model agrees well with ours for free-stream turbulence levels at 1-6%.

## Acknowledgements

My first and largest thanks goes to my supervisor Dan Henningson for always believing in me and giving me the opportunity to work in the fascinating field of fluid mechanics. His deep physical insight and wide knowledge in the field were always of great assistance. He also introduced me to an number of people without whom this thesis would have been incomplete.

Ardeshir Hanifi spent endless effort helping me to stabilise the PSEs. He has been a great help guiding me through the pit holes of the different research tools such as Latex, fortran and xmgr.

Martin Berggren introduced me to his world of adjoint equations and different inner-product spaces. He has always been there to share his vast research skills as well as his linguistic knowledge.

Alessandro Bottaro provided a very nice atmosphere in Toulouse when I was given the opportunity to spend the spring and autumn of 1998 there. He also greatly assisted me when learning about the secondary instability of streaks.

Casper Hildings spend hours discussing different, at the time interesting, subjects. Not always concerning fluid mechanics.

I wish to thank all the people working at the Department of Mechanics at KTH and at B-department at FFA for providing a nice and warm atmosphere.

Tack Linda, för kärlek, tålamod, hjälp och stöd.

## **Bibliography**

- [1] ABU-GHANNAM, B. J. & SHAW, R. 1980 Natural transition of boundary layers the effects of turbulence, pressure gradient, and flow history. J. Mech. Eng. Sci. 22, 213-228.
- [2] ALFREDSSON, P. H. & MATSUBARA, M. 1996 Streaky structures in transition In Proc. Transitional Boundary Layers in Aeronautics. (ed. R. A. W. M. Henkes & J. L. van Ingen), pp. 373-386, Royal Netherlands Academy of Arts and Sciences. Elsevier Science Publishers.
- [3] ANDERSSON, P. 1999 On the modelling of streamwise streaks in the Blasius boundary layer. TRITA-MEK, Technical Report 1999:14, Dept. of Mechanics, KTH, Stockholm, Sweden.
- [4] Andersson, P., Berggren, M. & Henningson, D. S. 1999 Optimal disturbances and bypass transition in boundary layers. *Phys. Fluids*. 11, 134-150.
- [5] Andersson, P., Bottaro, A., Henningson, D. S. & Luchini, P. 1999 Secondary instability of boundary layer streaks based on the shape assumption. TRITA-MEK, Technical Report 1999:13, Dept. of Mechanics, KTH, Stockholm, Sweden.
- [6] ANDERSSON, P., BRANDT, L., BOTTARO, A. & HENNINGSON, D. S. 1999 On the breakdown of boundary layer streaks. submitted to J. Fluid Mech.
- [7] Andersson, P., Henningson, D. S. & Hanifi, A. 1998 On a stabilization procedure for the parabolic stability equations. J. Eng. Math. 33, 311-332.
- [8] BERLIN, S., LUNDBLADH, A. & HENNINGSON, D. S. 1994 Spatial simulations of oblique transition in a boundary layer. Phys. Fluids. 6, 1949-1951.
- [9] BERLIN, S., WIEGEL, M. & HENNINGSON, D. S. 1999 Numerical and experimental investigations of oblique boundary layer transition. J. Fluid Mech. 393, 23-57.
- [10] BERTOLOTTI, F. P. 1991 Linear and Nonlinear Stability of Boundary Layers with Streamwise Varying Properties. PhD. Thesis, The Ohio State University, Department of Mechanical Engineering, Columbus, Ohio.
- [11] BERTOLOTTI, F. P. & HERBERT T. 1987 Stability analysis of nonparallel boundary layers. Bull. Am. Phys. Soc. 32, 2079.
- [12] BERTOLOTTI, F. P., HERBERT, T. & SPALART, P. R. 1992. Linear and nonlinear stability of the Blasius boundary layer. J. Fluid Mech. 242, 441-474.
- [13] BUTLER, K. M. & FARRELL, B. F. 1992 Three-dimensional optimal perturbations in viscous shear flow. Phys. Fluids A. 4, 1637-1650.
- [14] DUNHAM, J. 1972 Prediction of boundary-layer transition on turbomachinery blades. AGARD AG 164 No. 3.
- [15] EL-HADY, N. M. 1991 Nonparallel instability of supersonic and hypersonic boundary layers. Phys. Fluids A. 3, 2164-2178.
- [16] Ellingsen, T. & Palm, E. 1975 Stability of linear flow. Phys. Fluids. 18, 487-488.
- [17] ELOFSSON, P. A. 1998 An experimental study of oblique transition in a Blasius boundary layer flow. TRITA-MEK, Technical Report 1998:4, Dept. of Mechanics, KTH, Stockholm, Sweden.

- [18] EMMONS, H. W. 1951 The laminar-turbulent transition in a boundary layer Part I. J. Aero. Sci. 18, 490-498.
- [19] FARRELL, B. F. 1988 Optimal excitation of perturbations in viscous shear flow. Phys. Fluids. 31, 2093-2102.
- [20] FJØRTOFT, R. 1950 Application of integral theorems in deriving criteria for instability for laminar flows and for the baroclinic circular vortex. Geofys. Publ., Oslo. 17, No. 6, 1-52.
- [21] GAPONOV, S. A. 1981 The influence of flow non-parallelism on disturbance development in the supersonic boundary layers. In Proc. 8-th Canadian Congr. of Appl. Mech., 673-674.
- [22] GASTER, M. 1974 On the effects of boundary-layer growth on flow stability. J. Fluid Mech. 66, 465–480.
- [23] GUSTAVSSON, L. H. 1991 Energy growth of three-dimensional disturbances in plane Poiseuille flow. J. Fluid Mech. 224, 241–260.
- [24] HAJ-HARIRI, H. 1994 Characteristics analysis of the parabolized stability equations. Stud. Appl. Math. 92, 41-53.
- [25] HALL, P. 1983 The linear development of Görtler vortices in growing boundary layers. J. Fluid Mech. 130, 41-58.
- [26] HALL, P. & HORSEMAN, N. J. 1991 The linear inviscid secondary instability of longitudinal vortex structures in boundary-layers. J. Fluid Mech. 232, 357-375.
- [27] HEISENBERG, W. 1924 Über Stabilität und Turbulenz von Flüssigkeitsströmen. Ann. d. Phys. 74, 577-627. [English translation NACA TM 1291(1951)].
- [28] HENNINGSON, D. S. 1987 Stability of parallel inviscid shear flow with mean spanwise variation. Tech. Rep. FFA-TN 1987-57. Aeronautical Research Institute of Sweden, Bromma.
- [29] HENNINGSON, D. S., LUNDBLADH, A. & JOHANSSON, A. V. 1993 A mechanism for bypass transition from localized disturbances in wall bounded shear flows. J. Fluid Mech. 250, 169–207.
- [30] HERBERT, T. 1983 Secondary instability of plane channel flow to subharmonic threedimensional disturbances. Phys. Fluids. 26, 871-874.
- [31] HERBERT, T. 1988 Secondary instability of boundary layers. Ann. Rev. Fluid Mech. 20, 487-526.
- [32] HERBERT T. 1991 Boundary-layer transition analysis and prediction revisited. AIAA Paper 91-0737.
- [33] HERBERT T. 1997 Parabolized Stability Equations. Ann. Rev. Fluid Mech. 29, 245-283.
- [34] HULTGREN, L. S. & GUSTAVSSON, L. H. 1981 Algebraic growth of disturbances in a laminar boundary layer. Phys. Fluids. 24, 1000-1004.
- [35] ITOH, N. 1986 The origin and subsequent development in space of Tollmien-Schlichting waves in a boundary layer. Fluid Dyn. Res. 1, 119-130.
- [36] JOSLIN, R. D., STREETT, C. L. & CHANG, C. L. 1993 Spatial direct numerical simulations of boundary-layer transition mechanisms: Validation of PSE theory. Theor. Comp. Fluid Dyn. 4, 271–288.
- [37] KACHANOV, Y. S. 1994 Physical mechanisms of laminar-boundary-layer transition. Ann. Rev. Fluid Mech. 26, 411-482.
- [38] KACHANOV, Y. S., KOZLOV, V. & LEVCHENKO, V. Y. 1977 Nonlinear development of a wave in a boundary layer. *Izv. Akad. Nauk SSSR, Mekh. Zhidk. Gaza.* 3, 49-53. (in Russian).
- [39] KLEBANOFF, P. S., TIDSTROM, K. D. & SARGENT, L. M. 1962 The three-dimensional nature of boundary layer instability. J. Fluid Mech. 12, 1.
- [40] KLEISER, L. & ZANG, T. A. 1991 Numerical simulation of transition in wall-bounded shear flows. Ann. Rev. Fluid Mech. 23, 495-537.
- [41] KREISS, H.-O. & LORENZ, J. 1989 Initial-Boundary Value Problems and the Navier-Stokes Equations. Academic Press, New-York.

- [42] LANDAHL, M. T. 1977 Dynamics of boundary layer transition and the mechanism of drag reduction. Phys. Fluids. 20, 55-63.
- [43] LANDAHL, M. T. 1980 A note on an algebraic instability of inviscid parallel shear flows. J. Fluid Mech. 98, 243-251.
- [44] LI, F. & MALIK, M. R. 1995 Mathematical nature of parabolized stability equations. In R. Kobayashi (ed.), Laminar-Turbulent Transition. Proc. 4th IUTAM Symposium Sendai/Japan, Springer-Verlag, Berlin. 205-212.
- [45] LI, F. & MALIK, M. R. 1996 On the nature of PSE approximation. Theor. Comp. Fluid Dyn. 8, 253-273.
- [46] LIBBY, P. A. & FOX, H. 1964 Some perturbation solutions in laminar boundary-layer theory. J. Fluid Mech. 17, 433-449.
- [47] LIN, C. C. 1944 On the stability of two-dimensional parallel flows. Proc. Nat. Acad. Sci. 30, 316-324.
- [48] LUCHINI, P. 1996 Reynolds number independent instability of the Blasius boundary layer over a flat surface. J. Fluid Mech. 327, 101-115.
- [49] LUCHINI, P. 1999 Reynolds-number-independent instability of the boundary layer over a flat plate surface. Part 2: Optimal perturbations. accepted J. Fluid Mech.
- [50] MACK, L. M. 1977 Transition Prediction and Linear Stability Theory In AGARD Conference Proceedings No. 224, NATO Paris, 1-1.
- [51] Matsubara, M. 1997 Private Communications, (Unpublished data received from experiments conducted 1995 in the MTL-windtunnel at the Department of Mechanics at the Royal Institute of Technology in Sweden.)
- [52] MORKOVIN, M. V. 1969 The many faces of transition. In Viscous Drag Reduction (Wells, C. S., editor). Plenum Press.
- [53] NISHIOKA, M., IIDA, S. & ICHIKAWA, Y. 1975 An experimental investigation of the stability of plane Poiseuille flow. J. Fluid Mech. 72, 731-751.
- [54] ORR, W. M. F. 1907 The stability or instability of the steady motions of a perfect liquid and of a viscous liquid. Part I: A perfect liquid. Part II: A viscous liquid. Proc. Roy. Irish Acad. 27, 9-138.
- [55] ORSZAG, S. A. 1971 Accurate solution of the Orr-Sommerfeld stability equation. J. Fluid Mech. 50, 689-703.
- [56] RAYLEIGH, J. W. S. 1880 On the stability, or instability, of certain fluid motions. Proc. Math. Soc. Lond. 11, 57-70.
- [57] REDDY, S. C. & HENNINGSON, D. S. 1993 Energy growth in viscous channel flows. J. Fluid Mech. 252, 209-238.
- [58] REYNOLDS, O. 1883 On the experimental investigation of the circumstances which determine whether the motion of water shall be direct or sinuous, and the law of resistance in parallel channels. Phil. Trans. Roy. Soc. Lond. 174, 935-982.
- [59] ROACH, P. E. & BRIERLEY, D. H. 1992 The influence of a turbulent free-stream on zero pressure gradient transitional boundary layer development. Part I: Test cases T3A and T3B. In O. Pironneau, W. Rodi, I.L. Ryhming, A.M. Savill, and T.V. Truong, editors, Numerical simulation of unsteady flows and transition to turbulence, Cambridge University Press, 303-316.
- [60] SARIC, W. S. & NAYFEH, A. H. 1975 Non-parallel stability of boundary-layer flows. Phys. Fluids. 18, 945-950.
- [61] SCHLICHTING, H. 1933 Zur Entstehung der Turbulenz bei der Plattenströmung. Nachr. Ges. Wiss. Göttingen, Math. Phys. Klasse, 181–208.
- [62] SCHLICHTING, H. 1935 Amplitudenverteilung und Energiebilanz der kleinen Störungen bei der Plattenströmung. Nachr. Ges. Wiss. Göttingen, Math. Phys. Klasse, Fachgruppe I, 1, 47-78.

- [63] SCHMID, P. 1998 Energy amplification of steady disturbances in growing boundary layers. In (U. Frisch ed.), Advances in Turbulence VII, Kluwer Academic Publishers, Dordrecht. 101–104.
- [64] SCHUBAUER, G. B. & SKRAMSTAD, H. F. 1947 Laminar boundary layer oscillations and the stability of laminar flow. J. Aero. Sci. 14, 69-78.
- [65] SIMEN, M. 1992 Local and nonlocal stability theory of spatially varying flows. In M.Y. Hussaini, A. Kumar and C.L. Streett (eds.), *Instability, Transition and Turbulence*, Springer-Verlag, New York. 181–201.
- [66] SIMEN, M. 1993 Lokale und nichtlokale Instabilität hypersonischer Grenzschichtströmungen. PhD. Thesis, DLR FB 93-31.
- [67] SMITH, A. M. O. & GAMBERONI, N. 1956 Transition, pressure gradient and stability theory. Technical Report ES 26388, Douglas Aircraft Co.
- [68] SOMMERFELD, A. 1908 Ein Beitrag zur hydrodynamischen Erklärung der turbulenten Flüssigkeitbewegungen. Atti. del 4. Congr. Internat. dei Mat. III, Roma, 116–124.
- [69] SQUIRE, H. B. 1933 On the stability of three-dimensional distribution of viscous fluid between parallel walls. Proc. Roy. Soc. Lond. A. 142, 621-628.
- [70] TIETJENS, O. 1925 Beiträge zur Entstehung der Turbulenz. Z. Angew. Math. Mech. 5, 200–217.
- [71] TOLLMIEN, W. 1929 Über die Entstehung der Turbulenz. Nachr. Ges. Wiss. Göttingen, 21–44. [English translation NACA TM 609(1931)]
- [72] TREFETHEN, L. N., TREFETHEN, A. E., REDDY, S. C. & DRISCOLL, T. A. 1993 Hydrodynamic stability without eigenvalues. Science 261, 578-584.
- [73] VAN DRIEST, E. R. & BLUMER, C. B. 1963 Boundary layer transition: Freestream turbulence and pressure gradient effects. AIAA J. 1, 1303-1306.
- [74] VAN INGEN, J. L. 1956 A suggested semiempirical method for the calculation of the boundary layer transition region. Technical Report VTH-74, Faculty of Aerospace Eng., Delft University of Technology.
- [75] WESTIN, K. J. A., BOIKO, A. V., KLINGMANN, B. G. B., KOZLOV, V. V. & ALFREDS-SON, P. H. 1994 Experiments in a boundary layer subject to free-stream turbulence. Part I. Boundary layer structure and receptivity. J. Fluid Mech. 281, 193–218.
- [76] WIEGEL, M. 1996 Experimentelle Untersuchung von kontrolliert angeregten dreidimensionalen Wellen in einer Blasius-Grenzschicht. PhD thesis, TH Hannover.
- [77] YANG, Z. Y. & VOKE, P. R. 1991 Numerical simulation of transition under turbulence. Technical Report ME-FD/91.01, University of Surrey, Dept. Mech. Eng.